Available online at BCREC website: https://bcrec.id

Bulletin of Chemical Reaction Engineering & Catalysis, 17 (4) 2022, 798-810

Research Article

Modeling and Simulation of Carbon Dioxide Gas Reactive Desorption Process with Piperazine Promoted Diethanolamine Solvent in Sieve Tray Column

Nur Ihda Farikhatin Nisa, Nabila Farras Balqis, Muhammad Anshorulloh Mukhlish, Ali Altway, M. Mahfud*

Department of Chemical Engineering, Faculty of Industrial Technology and System Engineering (INDSYS), Institut Teknologi Sepuluh Nopember, Kampus ITS Sukolilo, Surabaya 60111, Indonesia.

Received: 23rd October 2022; Revised: 23rd November 2022; Accepted: 24th November 2022
Available online: 7th December 2022; Published regularly: December 2022

Abstract

Carbon dioxide (CO_2) is an acidic and corrosive gas, and the presence of this gas in the piping system can cause various problems in the industrial sector. Therefore, the CO_2 must be separated from the gas stream. One of the CO_2 gas separation processes from the gas stream is carried out in a CO_2 removal unit, where a desorption unit serves as a solvent regeneration step. Therefore, this study aims to develop a rate-based model and simulation of the reactive desorption process of CO_2 gas in a sieve tray column. The rate-based model in the reactive desorption process of CO_2 gas is based on film theory, the liquid in the tray is assumed completely agitated due to gas bubbling, the flow pattern of gas is plug flow, and the effect of the reaction on the mass transfer follows the enhancement factor concept. The number of trays used in this study was 20. In addition, the effect of several variables, such as: desorber pressure, rich amine temperature, rich amine flow rate, and reboiler load, was also assessed on the CO_2 stripping efficiency. The accuracy of our prediction model is 1.34% compared with industrial plant data. Compared with the chemical engineering simulator simulation results, the average deviation is 4%.

Keywords: Desorption; Diethanolamine; Rate-based model; Stripper; Tray column

How to Cite: N.I.F. Nisa, N.F. Balqis, M.A. Mukhlish, A. Altway, M. Mahfud. (2022). Modeling and Simulation of Carbon Dioxide Gas Reactive Desorption Process with Piperazine Promoted Diethanolamine Solvent in Sieve Tray Column. *Bulletin of Chemical Reaction Engineering & Catalysis*, 17(4), 798-810 (doi: 10.9767/bcrec.17.4.16245.798-810)

Permalink/DOI: https://doi.org/10.9767/bcrec.17.4.16245.798-810

1. Introduction

Carbon dioxide (CO_2) makes up most of the greenhouse gas emitted from human activities. Burning fossil fuels and deforestation have contributed to the rising level of CO_2 in the atmosphere. In July 2022, the atmospheric CO_2 level reached 419 ppm [1]. Excessive CO_2 emissions include various problems, such as climate change and global warming [2–5]. The industrial and agricultural sectors are among the significant contributors to the CO_2 emissions emitted through their power generation and natural gas processing units [6]. Due to its acidic and corrosive nature, CO_2 also causes damage to the industrial piping system and utilities. The presence of CO_2 in the gas streams can affect the plant performance resulting in problems, such as the low calorific value of natural gas and piping blockage of refineries at low temperatures [7,8].

Thus, various efforts have been made to reduce and suppress CO_2 gas emissions. One of the technologies currently being developed by researchers is Carbon Capture and Utilization

* Corresponding Author.
Email: mahfud@chem-eng.its.ac.id (M. Mahfud);
Telp: +62-31-5946240, Fax: +62-31-5999282

(CCU). This technology converts the recovered CO_2 gas from the CO_2 removal unit into new substances or products that the industry can reuse.

Most CO_2 removal units in the industry use chemical solvent absorption accompanied by a desorption unit as a solvent regeneration step. However, solvent regeneration is the step that requires the highest cost in the process of separating CO_2 from the gas stream, which can reach 80% of the total cost of CO_2 separation [9]. For this reason, modeling and simulation steps are needed to determine the best performance in minimizing operating costs and reducing energy requirements for solvent regeneration.

Apart from the cost factor, another factor that needs to be considered is the solvent's capacity to separate CO_2 gas from the gas stream. Potassium carbonate (K_2CO_3) and alkanolamine solvents are the most widely used solvents. However, using K_2CO_3 solvent in the CO_2 gas separation process is constrained by the slow reaction and the need for expensive equipment.

Alkanolamine solvents are commonly used for CO_2 removal from gas streams. Reports show that alkanolamine has several advantages, including high CO_2 absorption capacity, slight reaction enthalpy with CO_2, and low heat loss [10]. In addition, alkanolamine solutions have been reported to absorb CO_2 gas [11–13]. Alkanolamines are classified into three groups: 1) primary amines, such as mono ethanolamine (MEA) and diglycol amine (DGA); 2) secondary amines, such as diethanolamine (DEA) and di-isopropanol amine (DIPA); and 3) tertiary amines, such as methyl diethanolamine (MDEA) [14]. DEA is preferable to the extensively used MEA due to its lower solvent degradation and corrosiveness even at high amine concentrations. DEA also has a higher CO_2 absorption capacity and lower energy requirements for solvent regeneration than MEA. However, a low reaction rate occurs when DEA is reacted without a promoter. Hence, a diamine compound such as piperazine (PZ) is used as a catalyst to increase the absorption capacity of CO_2 and accelerate the reaction rate of DEA with CO_2 gas [15].

Modeling and simulation of the reactive absorption of CO_2 gas in alkanolamine solvents on tray columns and packed columns have been developed in previous studies [7,16–21], but the number of studies on desorption process reported in the literature is limited. In previous studies, modeling and simulation of the reactive desorption process of CO_2 gas were carried out on packed columns, both on a laboratory scale [22] and an industrial scale [9,23,24]. In addressing mass transfer in stripper, some authors in previous studies used the equilibrium stage [25], rate-based model [26–29], mass transfer with reaction in the liquid boundary layer and diffusion of reactants and products [22]. In completing the reactive desorption model, the author in previous studies used an in-house simulator [30], g-PROMS software [31], Aspen Plus [27,32,33], Aspen RateFrac [26], Aspen Custom Modeler [25], and MATLAB [23,34].

In previous studies, modeling and simulation of the reactive desorption process of CO_2 gas were carried out on packed columns in various solvents, such as K_2CO_3 [35], PZ [32], MEA [36], and MDEA [34], without considering other unreacted gases contained in the feed. Therefore, this study aims to develop a rate-based model and simulation of the reactive desorption process of CO_2 gas with piperazine-promoted DEA solvent in a sieve tray column by considering the presence of other unreacted gases in the feed (rich amine). The rate-based model in the reactive desorption process of CO_2 gas is based on film theory, the liquid in the tray is assumed completely agitated due to gas bubbling, the flow pattern of gas is plug flow, and the effect of the reaction on the mass transfer coefficient follows the enhancement factor concept. In addition, the effect of several variables, such as desorber pressure, rich amine temperature, rich amine flow rate, and reboiler load, was also assessed on the CO_2 stripping efficiency. The simulation results can be used to estimate the energy requirements for the CO_2 desorption process and optimize it to minimize the operating cost of the CO_2 removal unit.

2. Materials and Methods

2.1 Reaction Kinetic and Absorption Rate

The reaction mechanism of CO_2 gas with DEA solvent follows the reaction in Equation (1) [37]. Meanwhile, the reaction mechanism of CO_2 gas with the PZ promoter follows the reaction in Equation (2) [38].

$$CO_2 + R_2NH \xleftrightarrow{k_{R_2NH}} R_2H^+HCOO^- \quad (1)$$

$$CO_2 + PZ + B \xleftrightarrow{K_1, k_{PZ}} PZCOO^- + BH^+ \quad (2)$$

B are several types of bases in the solution, namely PZ, $PZCOO^-$, PZH^+, H_2O, and OH^-. The reaction rate constant (k_{R2NH} and k_{PZ}) in Equations (1) and (2) are determined from Equations (3) and (4) that correlated with temperature (T, Kelvin).

$$\ln k_{R_2NH} = 27.06 - \frac{5284.4}{T} \quad (3)$$

$$\ln k_{PZ} = 32.52 - \frac{6433.73}{T} \quad (4)$$

The equilibrium reaction in the solution is shown in Equations (5)-(11) below [39]:

$$CO_2 + 2R_2NH \xleftrightarrow{K_C} R_2NCOO^- + R_2NH_2^+ \quad (5)$$

$$H_2O + R_2NCOO^- \xleftrightarrow{K_{eq}} R_2NH + HCO_3^- \quad (6)$$

$$R_2NH_2^+ \xleftrightarrow{K_b} R_2NH + H^+ \quad (7)$$

$$PZ + H^+ \xleftrightarrow{K_2} PZH^+ \quad (8)$$

$$CO_2 + H_2O \xleftrightarrow{K_3} HCO_3^- + H^+ \quad (9)$$

$$HCO_3^- \xleftrightarrow{K_4} CO_3^{2-} + H^+ \quad (10)$$

$$H_2O \xleftrightarrow{K_w} H^+ + OH^- \quad (11)$$

Equilibrium constants (K) in Equation (5) can be obtained from the other equilibrium constants by following Equation (12):

$$K_C = \frac{K_3}{K_b K_{eq}} \quad (12)$$

The value of the reaction equilibrium constant for Equations (2) and (8) used Equations (13) and (14) [40]. Meanwhile, Equations (6), (7), and (9) used Equations (15), (16), and (17) [41]. The value of the reaction equilibrium constant for Equations (10) and (11) follows Equations (18) and (19) [37].

$$K_1 = \exp\left(466.497 + \frac{1614.5}{T} - 97.540\ln T + 0.2471T\right) \quad (13)$$

$$\frac{1}{K_2} = \exp\left(514.314 - \frac{34910.9}{T} - 74.602\ln T\right) \quad (14)$$

$$K_{eq} = \exp\left(4.825 - \frac{1885}{T}\right) \quad (15)$$

$$K_b = \exp\left(-2.551 - \frac{5652}{T}\right) \quad (16)$$

$$K_3 = \exp\left(\begin{array}{l} -241.818 + \frac{298.253\times10^3}{T} - \frac{148.528\times10^6}{T^2} \\ + \frac{332.648\times10^8}{T^3} - \frac{282.394\times10^{10}}{T^4} \end{array}\right) \quad (17)$$

$$K_4 = \exp\left(\begin{array}{l} -294.74 + \frac{364.385\times10^3}{T} - \frac{184.158\times10^6}{T^2} \\ + \frac{415.793\times10^8}{T^3} - \frac{354.291\times10^{10}}{T^4} \end{array}\right) \quad (18)$$

$$K_w = \exp\left(\begin{array}{l} 39.5554 - \frac{987.9\times10^2}{T} + \frac{568.828\times10^5}{T^2} \\ - \frac{146.451\times10^8}{T^3} + \frac{136.146\times10^{10}}{T^4} \end{array}\right) \quad (19)$$

2.2. Gas Solubilities

The solubility of CO_2 gas in the promoted DEA solution follows the rules of Henry's law. The concentration of CO_2 at the interface ($C_{CO2,i}$ kmole.m^{-3}) was calculated by Equation (20) [42]. Since the reaction was a fast pseudo-first-order reaction, the enhancement factor (E) was calculated from Equation (21) [42] with the value of k_1 is shown in Equation (22) [42].

$$C_{CO_2,i} = \frac{k_G y_{CO_2} P + E k_L C_{CO_2,e}}{E k_L + k_G H_e} \quad (20)$$

$$E = \frac{\sqrt{k_1 C_B^0 D_A}}{k_L} \quad (21)$$

$$k_1 = k_{DEA} C_{DEA} + k_{PZ} C_{PZ} \quad (22)$$

Here, k_G, k_L, k_1, y_{CO2}, P, $C_{CO2,e}$, H_e, C_B^0, D_A are the mass transfer coefficient of the gas phase (kmole.m^2.s^{-1}), mass transfer coefficient of the liquid phase (kmole.m^2.s^{-1}), constant of the pseudo-first-order reaction (s^{-1}), mole fraction of CO_2 in the gas phase, pressure (atm), equilibrium concentration of CO_2 in liquid phase (kmole.m^{-3}), Henry's constant, concentration of reactant B in the liquid body (kmole.m^{-3}), and diffusivity (m^2.s^{-1}), respectively.

The gas solubility in the electrolyte solution was estimated by the method of Van Krevelen and Hoftijzer. This method corresponds to Henry's constant (H_e) in solution, calculated by Equations (23), (24), (25), and (26) [8].

$$\log\left(\frac{H_e}{H_e^0}\right) = \sum hl \quad (23)$$

$$H_{e,T}^0 = H_{e,298.15}^0 \exp\left[\frac{-d\ln H}{d\left(\frac{1}{T}\right)}\left(\frac{1}{T} - \frac{1}{298.15}\right)\right] \quad (24)$$

$$I = \frac{1}{2}\sum C_i z_i^2 \quad (25)$$

$$h = h_+ + h_- + h_G \quad (26)$$

In this equations, H_e^0, h, I, C_i, h_+, h_-, h_G, h_T are Henry's constant of component in pure water with temperature T (Pa.m^3.kmole^{-1}), ion specific parameter (m^3.kmole^{-1}), ionic strength in solution (g ion/liter), molar concentration of component (kmole.m^{-3}), cation specific parameter (m^3.kmole^{-1}), anion specific parameter (m^3.kmole^{-1}), gas specific parameter (m^{3}kmole^{-1}), and temperature correction (m^3.kmole^{-1}.K^{-1}), respectively. The value of h_G was calculated by Equation (27) [43].

$$h_G = h_{G,0} + h_T\left(T - 298.15\right) \quad (27)$$

Values of $H^0_{e,298.15}$ and $-d \ln H/d(1/T)$ can be seen in Table 1 [44]. Meanwhile, the values of $h_{G,0}$ (gas specific parameter at 298 K, $m^3.kmole^{-1}$) and h_T on each component is presented in Table 2 [45].

2.3 Mass and Heat Transfer Coefficient

The estimation of the diffusion coefficient in the mixture (D_L and D_G) was predicted using the Wilke-Chang equation for liquids (28) [43] and Fuller's equation for gases (29) [42].

$$D_L = 7.4\times10^{-8}\frac{\left(\Phi M_{H_2O}\right)^{0.5}T}{\mu_{H_2O}v_i^{0.6}} \quad (28)$$

$$D_G = 10^{-7}T^{-1.75}\frac{\left(\frac{1}{M_A}+\frac{1}{M_B}\right)^{0.5}}{P\left(\left(\sum v_A\right)^{1/3}+\left(\sum v_B\right)^{1/3}\right)^2} \quad (29)$$

In this equations, Φ, M_i, μ, v are association factor for solvent (2.6 for water), molecular weight of component ($kg.kmole^{-1}$), viscosity (Pa.s), and molar volume of component ($m^3.kmole^{-1}$), respectively.

The mass transfer coefficient of the gas phase k_G in the CO_2 gas desorption process on the sieve tray column ranged from 1 to 4.5×10^{-4} $cm.s^{-1}$ [43] The mass transfer coefficient of the liquid phase k_L was calculated using Equation (30) [43], while the surface area of the interface (a) was determined by Equation (31) [43].

$$k_L = o.31\left(gv\right)^{1/3}\left(\frac{D_L}{v}\right)^{2/3} \quad (30)$$

$$a = 0.38\left(\frac{\mu}{\mu_t}\right)^{0.775}\left(\frac{\mu\rho}{nd\mu}\right)^{0.125}\left(\frac{g\rho}{d\sigma}\right)^{1/3} \quad (31)$$

Here, g, d, ρ, σ are gravity acceleration ($m.s^{-2}$), tray hole diameter (m), density ($kg.m^{-3}$), solvent surface tension ($dyne.cm^{-1}$), respectively.

2.4 Mathematical Model

The mathematical model used to simulate the reactive desorption process of CO_2 gas in piperazine-promoted DEA solvent on a sieve tray column was based on mass and heat balances for the liquid and gas components arranged to form a non-linear algebraic system equation. The model used was a rate-based model with several assumptions: CO_2 gas reactive desorption process in steady state; the desorption column is in adiabatic condition; the interfacial surface area is the same for mass and heat transfer processes; the reaction is fast and pseudo first order; the heat transfer resistance in the liquid phase is smaller than in the gas phase; the surface temperature is the same as the bulk temperature; the liquid and gas phases are in ideal mixed conditions; CO_2 gas reacts with DEA to produce non-volatile products; the liquid in the tray is assumed completely agitated due to gas bubbling, and the flow pattern of gas is plug flow; the content of rich amine, which includes acid gas, is only CO_2 without H_2S. The CO_2 removal unit studied is located after the SRU unit; the gas leaving the condenser is saturated with water vapor; the composition of the rich amine stream not only contains CO_2 gas, but also considers the solubility of other gases, including methane, ethane, propane, n-butane, n-pentane, hexane, and nitrogen.

The design of the CO_2 gas desorption unit used in this study is shown in Figure 1. This figure shows that the rich amine from the CO_2 gas reactive absorption process was used as a feed for the CO_2 gas reactive desorption process. The mechanism of mass and heat transfer processes in the sieve tray column in the reactive desorption process of CO_2 gas is presented in Figure 2. From this figure, the equation for the overall mass balance for the liquid and gas phases is determined from Equations (32) and (33). Meanwhile, the equation for the mass bal-

Table 1. Value of Henry's constant component at the temperature of 298.15 K.

Component	$He^0_{298,15}$ ($mole.m^{-3}.Pa^{-1}$)	$-d \ln H/d(1/T)$ (K)
CO_2	3.3×10^{-4}	2400
N_2	6.4×10^{-6}	1300
CH_4	1.4×10^{-5}	1600
C_2H_6	1.9×10^{-5}	2400
C_3H_8	1.5×10^{-5}	2700
C_4H_{10}	1.2×10^{-5}	3100
C_5H_{12}	8.0×10^{-6}	3400
C_6H_{14}	6.1×10^{-6}	3800

Table 2. Values of h_G and h_T for each component.

Component	$h_{G,0}$ (10^{-6}) ($cm^3.mole^{-1}$)	h_T (10^{-6}) ($cm^3.mole^{-1}.K^{-1}$)
CO_2	−17.2	−0.338
N_2	−1	−0.605
CH_4	2.2	−0.524
C_2H_6	12	−0.601
C_3H_8	24	−0.702
C_4H_{10}	29.7	−0.815
C_5H_{12}	33.5	−0.922
C_6H_{14}	37.1	−0.971

ance for the liquid phase on the tray (34-35) and the mass balance for the gas phase (36-37) was obtained.

$$L_{out}X_{out} = \left(1 - E_S\right)L_{in}X_{in} \quad (32)$$

$$G_1 Y_{CO_2,1} = G_{N+1}Y_{CO_2,N+1} + E_S L_{in}X_{in} \quad (33)$$

$$L_{k-1} + N_{k,CO_2}aV = L_k \quad (34)$$

$$L_{k-1}X_{k-1,CO_2} + N_{k,CO_2}aV = L_k X_{k,CO_2} \quad (35)$$

$$G_{k+1} = G_k + N_{k,CO_2}aV \quad (36)$$

$$G_{k+1}Y_{k+1,CO_2} = G_k Y_{k,CO_2} + N_{k,CO_2}aV \quad (37)$$

Here, k, L, X, E_S, G, Y, $N_{k,CO2}$ are tray number, mass of liquid (kgmole.m^{-3}), liquid fraction of component, stripping efficiency (%), mass of gas (kgmole.m^{-3}), gas fraction of component, and mass transfer flux of CO_2 (kmole.m^2.s^{-1}), respectively.

Aside from the mass transfer process, a heat transfer occurred in the reactive desorption process of CO_2 gas. The heat balance equations in the liquid and gas phases in the sieve tray column are described in Equations (38) and (39). Here, (ΔH) and (ΔH_r) are the sensible heat of each component (J.kmole^{-1}) and heat of reaction (J.kmole^{-1}).

$$L_{k-i}\Delta H_{L,k-i} + \left(N_{k,CO_2}\Delta H_{k,CO_2} + N_{k,H_2O}H^V_{H_2O}\right)aV = L_k\Delta H_{L,k} + N_{k,CO_2}\Delta H_{r,CO_2} + h_G aV\left(T_G - T_L\right) \quad (38)$$

$$G_{k+1}\Delta H_{G,k+1} + h_G aV\left(T_G - T_L\right) = G_k\Delta H_{G,k} + \left(N_{k,CO_2}\Delta H_{k,CO_2} + N_{k,H_2O}H^V_{H_2O}\right)aV \quad (39)$$

The equation for the mass and energy balance for the condenser (40-42) and for the reboiler (43-45) was obtained. Here, D, B, Q_C, Q_{reb} are mass of distillate (kgmole.m^{-3}), mass of bottom product (kgmole.m^{-3}), condenser load (kW), and reboiler load (kW).

$$G_1 = D + G_0 \quad (40)$$

$$G_1 Y_{1,i} = DX_{D,i} + G_0 Y_{0,i} \quad (41)$$

$$G_1\Delta H_{G_1} = D\Delta H_D + G_0\Delta H_{G_0} + Q_C \quad (42)$$

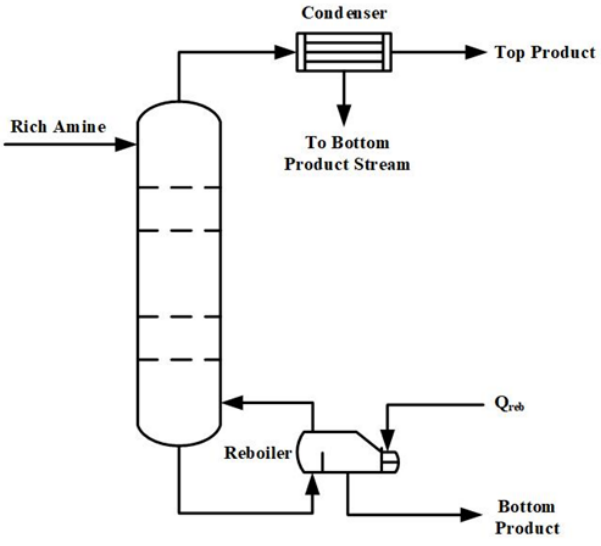

Figure 1. Schematic diagram of CO_2 gas desorption process.

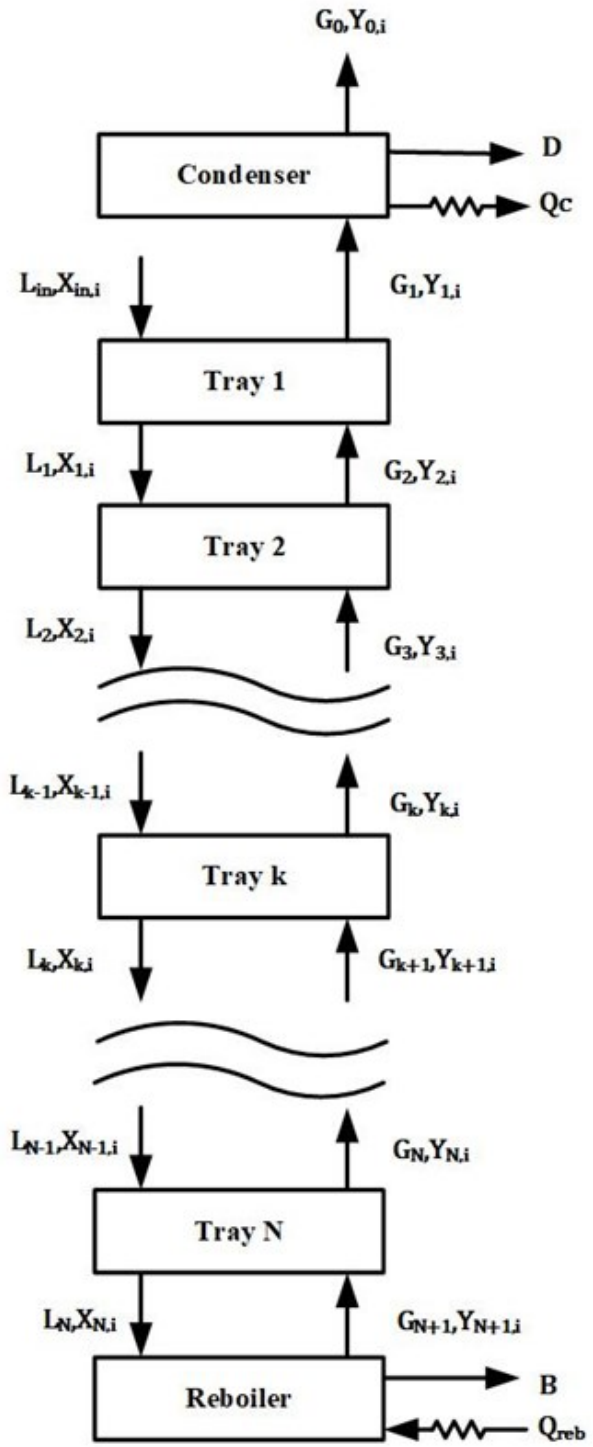

Figure 2. Mechanism of CO_2 gas reactive desorption process.

$$L_N = B + G_{N+1} \quad (43)$$

$$L_N X_{N,i} = BX_{B,i} + G_{N+1} Y_{N+1,i} \quad (44)$$

$$L_N \Delta H_{L,N} + Q_{reb} = B\Delta H_B + G_{N+1} \Delta H_{G_{N+1}} \quad (45)$$

The mass transfer flux of CO_2 ($N_{k,CO2}$) from liquid to gas (stripping CO_2 on tray-k) uses the transport interface approach and the enhancement factor concept defined in Equation (46). The mass transfer flux for H_2O ($N_{k,H2O}$) from gas to liquid uses the transport interface approach, which is shown in Equation (47). Where, the value of $C_{CO2,i}$ in Equation (46) is obtained from Equation (20). The heat of reaction (ΔH_r) was determined by Equation (48). Meanwhile, the sensible heat of each component (ΔH) was calculated by Equation (49).

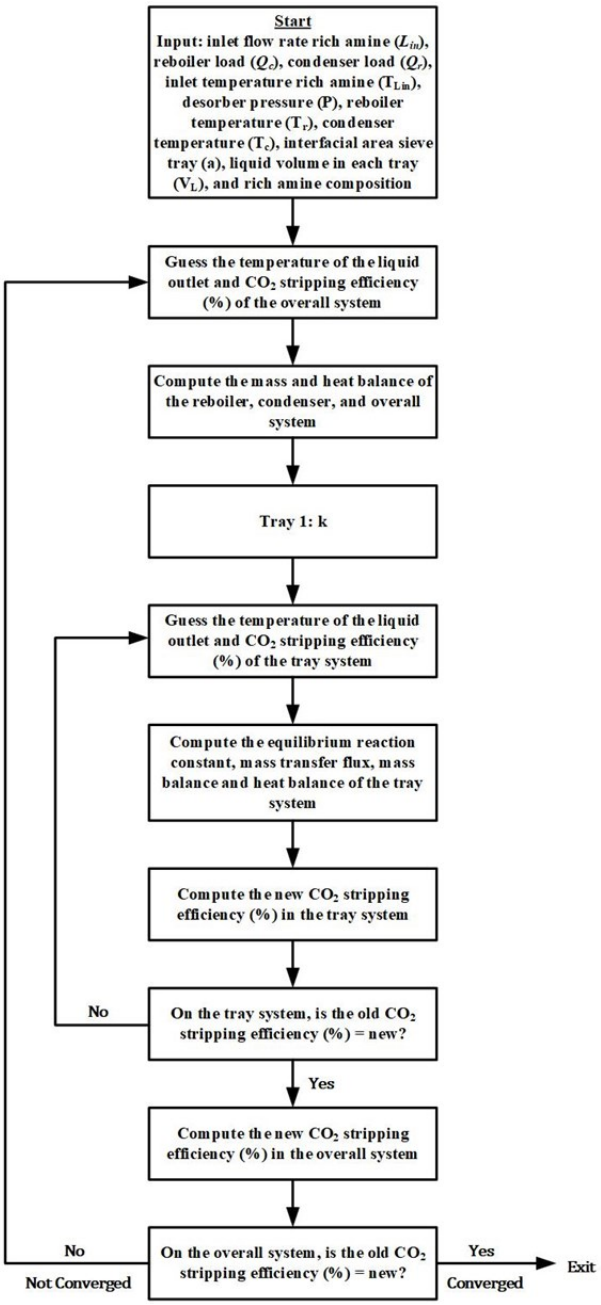

Figure 3. Algorithm of numerical calculation for the CO_2 desorption process.

$$N_{k,CO_2} = k_{L,CO_2} E\left(C_{CO_2,e} - C_{CO_2,i}\right) \quad (46)$$

$$N_{k,H_2O} = k_{G,H_2O}\left(P^S_{H_2O} - P_{H_2O}\right) \quad (47)$$

$$\Delta H_r = \Delta H_{desorption} \quad (48)$$

$$\Delta H = \int C_P dT \quad (49)$$

In addition, the heat of condensation of water (ΔH^V) was generated by linear interpolation of the steam table, and the heat transfer coefficient of water vapor was determined to be 125 $W.m^{-2}.K^{-1}$ from 100-1000 $W.m^{-2}.K^{-1}$.

Ion concentration (C) in the solution in the tray can be determined from equilibrium restriction in Equations (50)–(57), charge balance in Equation (58), and amine balance in Equations (59)–(60).

$$K_C = \frac{C_{DEACOO^-} C_{DEAH^+}}{C_{CO_2} C^2_{DEA}} \quad (50)$$

$$K_{eq} = \frac{C_{DEA} C_{HCO_3^-}}{C_{H_2O} C_{DEACOO^-}} \quad (51)$$

$$K_b = \frac{C_{DEA} C_{H^+}}{C_{DEAH^+}} \quad (52)$$

$$K_1 = \frac{C_{PZCOO^-} C_{H^+}}{C_{CO_2} C_{PZ}} \quad (53)$$

$$K_2 = \frac{C_{PZH^+}}{C_{PZ} C_{H^+}} \quad (54)$$

$$K_3 = \frac{C_{HCO_3^-} C_{H^+}}{C_{CO_2,e}} \quad (55)$$

$$K_4 = \frac{C_{CO_3^{2-}} C_{H^+}}{C_{HCO_3^-}} \quad (56)$$

$$K_W = C_H + C_{OH^-} \quad (57)$$

$$C_{PZH^+} + C_{DEAH^+} + C_{H^+} = C_{OH^-} + C_{HCO_3^-} + C_{CO_3^{2-}} \quad (58)$$

$$C_{DEA,in} = C_{DEA} + C_{DEAH^+} \quad (59)$$

$$C_{PZ,in} = C_{PZ} + C_{PZH^+} + C_{PZCOO^-} \quad (60)$$

2.5 Numerical Solution

The system of linear algebraic equations developed previously was solved numerically by Successive Approximation methods using the iterative variable percent stripping CO_2. The calculation is carried out in the following steps: The calculation begin with determination of

flow rate of water vapor generated from reboiler using reboiler energy balance (Equation (45)). Next, a trial percent stripping of total CO_2, it continues calculating the overall system mass balance (Equations (32) and (33)) to determine the liquid and gas outflow condition. After that, the mass (Equations (34) and (35)) and energy balances (Equations (36) and (37)) are calculated for each tray, starting from the first tray. In calculating the mass balance per tray, the percent stripping of CO_2 on the tray is corrected from the mass transfer calculation. Percent stripping CO_2 overall can be checked from the calculated percent stripping CO_2 overall obtained from the stage-to-stage calculation. This numerical solution is carried out by creating a program in MATLAB R2020a. Algorithm of numerical calculation for the CO_2 desorption process can be seen in Figure 3.

2.6 Model Validation

The simulation results were compared with industrial data plant and ASPEN HYSYS V11. The deviation of the computation results with ASPEN HYSYS V11 computation was determined as Root-mean-square deviation (RMSD) in Equation (61) with CO_2 stripping efficiency in MATLAB R2020a (E_S^M) and CO_2 stripping efficiency in ASPEN HYSYS V11 (E_S^H).

$$RMSD = \sqrt{\frac{\sum\left(E_S^M - E_S^H\right)^2}{\sum\left(E_S^H\right)^2}} \tag{61}$$

3. Results and Discussion

The developed model was used to simulate the performance of an industrial sieve tray column with diameter of 118.872 cm, weir height of 3.95 cm and number tray of 20. This research was carried out by making mathematical modeling and process simulations to remove CO_2 gas from a liquid mixture consisting of several components in Table 3. The column pressure was varied from 1.5 to 3 bar. The inlet rich amine temperature varied from 343.15 K to 358.15 K. The inlet rich amine flow rate varied from 7 $m^3.hour^{-1}$ to 10 $m^3.hour^{-1}$. The reboiler load varied from 3,000 kW to 4,500 kW. With the amount of CO_2 feed in the desorber of 0.54 $kmole.m^{-3}$ (Table 3) and rich amine flow rate 10 $m^3.hour^{-1}$, the reboiler load variable (3,000 kW to 4,500 kW) can be converted to 45,455 kJ/kg of CO_2 to 68,182 kJ/kg of CO_2. The variable values are determined from the operation of the existing CO_2 removal plant in industry. This study also employed a rate-based model with an enhancement factor approach. The reactive desorption process occurred in a sieve tray column, so the mathematical modeling focused on the tray's mass and heat transfer process, chemical reactions, and thermodynamics.

Several operating variables were then reviewed for their effect on the CO_2 stripping efficiency, such as desorber pressure, rich amine temperature, rich amine flow rate, and reboiler load. The fast and pseudo first order assumption was validated by determining the value of Hatta Number (H_a) and instantaneous enhancement factor in each tray and check the following Equation (62) satisfied [43].

$$3 < H_a < 0.5E_i \tag{62}$$

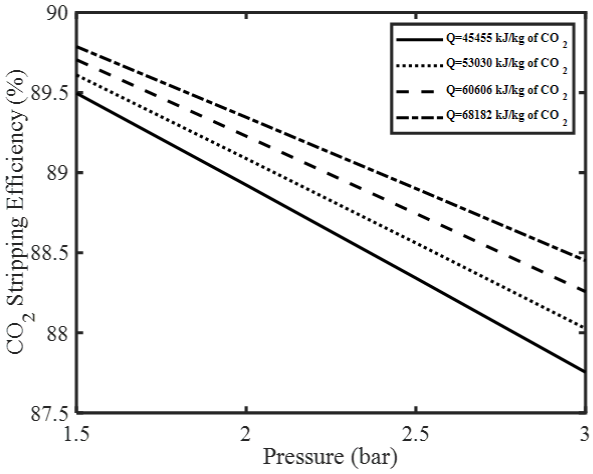

Figure 4. The effect of desorber pressure on CO_2 stripping efficiency.

Table 3. Inlet liquid composition.

Component	Composition ($kmole.m^{-3}$)
DEA	2.3982
DEACOO	0.47468
DEAH	0.47468
HCO_3	0.049156
H	1.2348×10^{-10}
OH	0.00012126
CO_3	0.010833
PZ	0.25669
PZH	0.092229
PZCOO	0.0012871
CH_4	0.0292
C_2H_6	0.0038
C_3H_8	0.0021
C_4H_{10}	0.00125
C_5H_{12}	0.000287
C_6H_{14}	0.0000665
N_2	0.000252

3.1 The Effect of Desorber Pressure on CO_2 Stripping Efficiency

Desorber pressure is one of the variables influencing the reactive desorption process of CO_2 gas. The effect of desorber pressure on CO_2 stripping efficiency is shown in Figure 4. From Figure 4, it can be seen that the higher the desorber pressure (ranging from 1.5 bar to 3 bars), the CO_2 stripping efficiency decreased by 1.74%. When the desorber pressure was 1.5 bar with a reboiler load of 45,455 kJ.kg^{-1} of CO_2, the stripping efficiency of CO_2 obtained was 89.496%. Meanwhile, when the desorber pressure was 3 bars, the stripping efficiency of CO_2 obtained was 87.75%. The decrease in CO_2 stripping efficiency with increasing pressure was due to the CO_2 solubility increase and then, the CO_2 gas absorbed in the solution is difficult to escape [42].

3.2 The Effect of Rich Amine Temperature on CO_2 Stripping Efficiency

The effect of rich amine temperature on CO_2 stripping efficiency is presented in Figure 5. In this figure, it can be seen that the increase in the rich amine temperature was directly proportional to the stripping efficiency of CO_2 gas. The higher the rich amine temperature (343.15 K to 358.15 K), the CO_2 stripping efficiency increased by 15.28%. At a pressure of 1.5 bar with a rich amine temperature of 343.15 K, the stripping efficiency of CO_2 obtained was 77.56%. Meanwhile, when the rich amine temperature was 358.15 K the CO_2 stripping efficiency was 92.84%. The increase in CO_2 stripping efficiency was due to the greater the rich amine temperature, the greater the reaction rate and the diffusivity of the solution, so the greater the concentration gradient close to the gas-liquid interface [9]. Increasing the rich amine temperature can also reduce the solubility of CO_2 gas in solution, where the smaller the gas solubility, the greater the resulting CO_2 stripping efficiency.

3.3 The Effect of Reboiler Load on CO_2 Stripping Efficiency

In the reactive desorption process of CO_2 gas, the reboiler serves to heat the solution to produce water and release the CO_2 that is still bound. The effect of reboiler load on CO_2 stripping efficiency is displayed in Figure 6. This figure shows that the higher the reboiler load (45,455 kJ.kg^{-1} of CO_2 to 68,182 kJ.kg^{-1} of CO_2), the greater the resulting CO_2 stripping efficiency. When reboiler load was 45,455 kJ.kg^{-1} of CO_2 with a desorber pressure of 1.5 bar; the CO_2 stripping efficiency was 89.50%. Meanwhile, at the same pressure with the reboiler load of 68,182 kJ.kg^{-1} of CO_2, the stripping efficiency of CO_2 was 89.78%. The increase in CO_2 stripping efficiency was due to the greater the reboiler load, the greater the steam mass required. The amount of steam added to the column greatly influenced achieving the desired level of separation [9]. The increase of reboiler load (or steam required) will increase the liquid temperature. This will decrease the CO_2 solubility in liquid and increase the separation efficiency. It led CO_2 gas absorbed in the piperazine-promoted DEA solution to be more easily released so that the resulting stripping efficiency was greater.

3.4 The Effect of Rich Amine Flow Rate on CO_2 Stripping Efficiency

Rich amine solution is produced from the CO_2 gas reactive absorption process and used

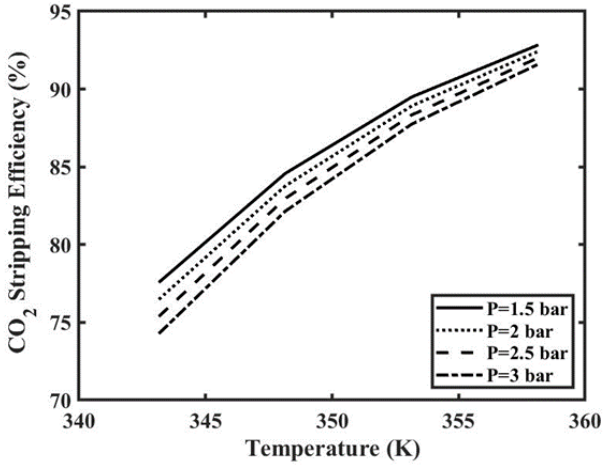

Figure 5. The effect of rich amine temperature on CO_2 stripping efficiency.

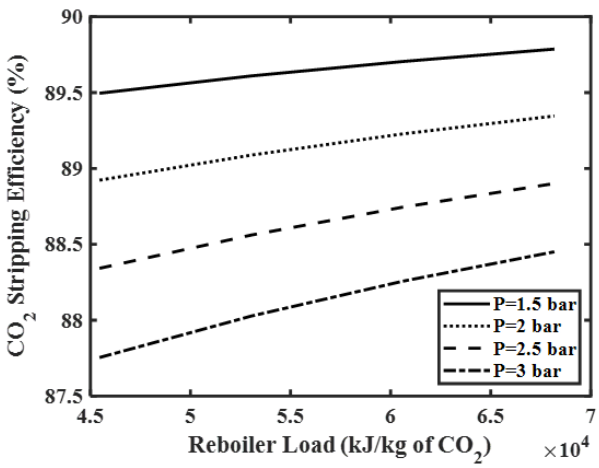

Figure 6. The effect of reboiler load on CO_2 stripping efficiency.

as a feed solution. This solution has a very large CO_2 content. Meanwhile, the effect of rich amine flow rate on CO_2 stripping efficiency is depicted in Figure 7.

From Figure 7, it can be seen that the increase in the rich amine flow rate was inversely proportional to the resulting CO_2 stripping efficiency. CO_2 stripping efficiency decreased by 3.29% from 92.78% to 89.50% in the rich amine flow rate range of 7 $m^3.hour^{-1}$ to 10 $m^3.hour^{-1}$, with a desorber pressure of 1.5 bar. It was because the greater the rich amine flow rate, the smaller the contact time of the solution in the sieve tray column so that the resulting CO_2 stripping efficiency decreased [23].

3.5 Distribution of Liquid and Gas Concentration in Sieve Tray Column

The distribution of the liquid phase concentration in the reactive desorption process of CO_2 gas in the sieve tray column is illustrated in Figure 8. From Figure 8, it can be seen that the DEA solution concentration increased from tray 1 to tray 20. DEA was regenerated from the reaction between $DEAH^+$ with $DEACOO^-$ and HCO_3^- so that the composition increased. The same thing also happened to PZ, which experienced an increase but was less significant. PZ was regenerated from the reaction between PZH^+ and HCO_3^-. Regenerated PZ reacted again with H^+ ions from the water dissociation, thus forming PZH^+. PZH^+ was also regenerated from the reaction between $PZCOO^-$ and H^+ ions. The 1st tray position showed the top tray position, and the 20th tray indicated the bottom tray position.

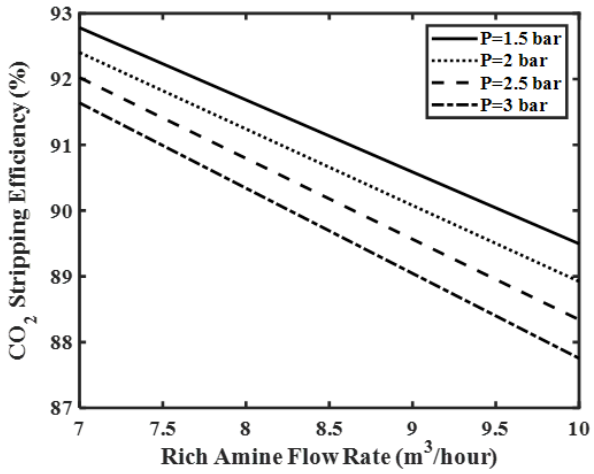

Figure 7. The effect of rich amine flow rate on CO_2 stripping efficiency.

The distribution of gas phase concentration on the sieve tray column is demonstrated in Figure 9. Unlike the liquid phase, the gas phase flowed from the bottom tray to the top tray. The position of the 1st tray showed the position of the top tray. From Figure 9, it can be seen that the concentration of CO_2 gas increased from 0.00045178 $kmole.m^{-3}$ to 0.005252600 $kmole.m^{-3}$. It was because the higher the composition of $DEACOO^-$, HCO_3^-, CO_3^{2-} and $PZCOO^-$ ions increased, the number of moles of CO_2 gas formed also increased.

The concentration of other dissolved gases, such as methane gas (CH_4), ethane gas (C_2H_6), propane gas (C_3H_8), and butane gas (C_4H_{10}), also increased. However, the increase in dissolved gases was less significant than the increase in CO_2 gas concentration in the sieve tray column. It was because when the rich amine solution flowed into the bottom tray, the solution would come into contact with steam from the reboiler so that the solution temperature would increase. Increasing the temperature would cause a decrease in the gas solubili-

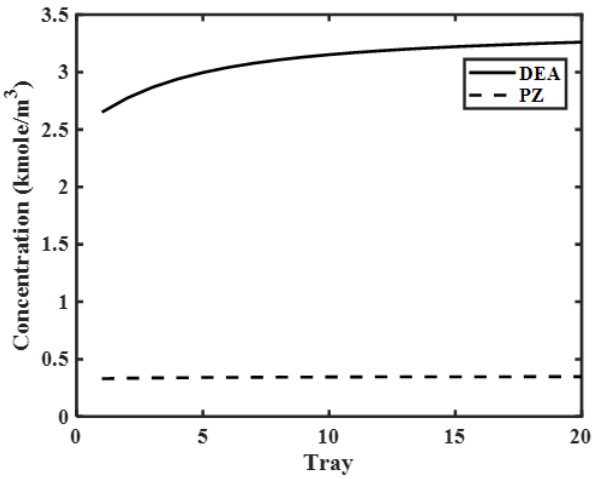

Figure 8. Distribution of DEA and PZ concentration in sieve tray column.

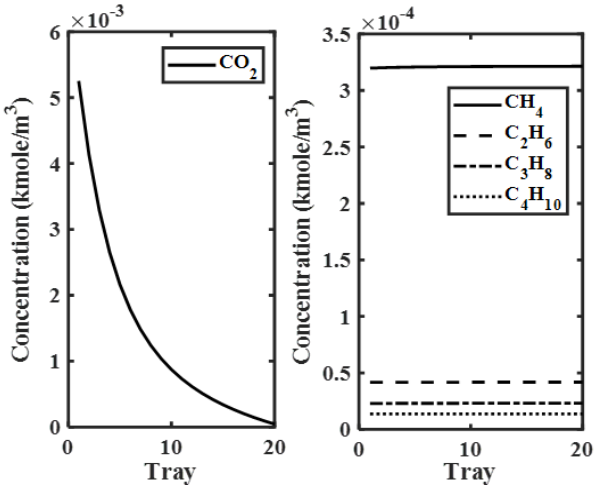

Figure 9. Concentration distribution of dissolved gases in sieve tray column.

ty so that the gas was to escape and flow to the top of the tray.

3.6 Model Validation

A comparison between the MATLAB R2020a simulation results and industrial plant data is used for model validation. Table 4 compares the MATLAB R2020a simulation results and industrial plant data. It can be seen from Table 4 that for the same operating conditions, the predicted CO_2 stripping efficiency is 88.35% compared to 89.68% in industrial plant data. The accuracy of our prediction model is 1.34% compared with industrial plant data.

Validation was also carried out with ASPEN HYSYS V11, where the average deviation between MATLAB R2020a and ASPEN HYSYS V11 was calculated using the Root-mean-square-deviation (RMSD) in Equation (61). The comparison between the MATLAB R2020a simulation results and the ASPEN HYSYS V11 simulation results is shown in Figure 10, with an average deviation of 4%.

4. Conclusion

In this research, a rate-based model of the reactive desorption process of CO_2 gas has been developed with piperazine-promoted DEA solvent in a sieve tray column. The number of trays used was 20. Several variables, such as desorber pressure, rich amine temperature, reboiler load, and rich amine flow rate, were also studied for their effect on CO_2 stripping efficiency. The higher the desorber pressure (ranging from 1.5 bar to 3 bar) the CO_2 stripping efficiency decreased by 1.74%. The higher the rich amine temperature (343.15 K to 358.15 K) the CO_2 stripping efficiency increased by 15.28%. CO_2 stripping efficiency increased by 0.29% in the reboiler load of 45,455 kJ.kg^{-1} of CO_2 to 68,182 kJ.kg^{-1} of CO_2. The CO_2 stripping efficiency decreased by 3.29% in the rich amine flow rate of 7 m^3.hour^{-1} to 10 m^3.hour^{-1}. The accuracy of our prediction model is 1.34% compared with industrial plant data. Compared with the ASPEN HYSYS V11 simulation results, the average deviation is 4%.

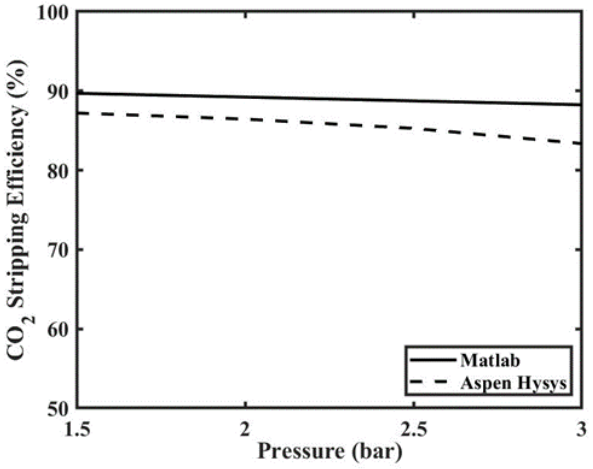

Figure 10. The effect of desorber pressure on CO_2 stripping efficiency.

Acknowledgments

Thanks to Indonesia Endowment Funds for Education (LPDP) through the Indonesia-Domestic Lecturer Excellence Scholarship Education Program (BUDI-DN) for research funding support (Grant number: 20200421681167).

Author Contributions: N. I. F. Nisa: Conceptualization, Methodology, Software, Validation, Investigation, Writing – Original Draft, Writing – Review & Editing; N. F. Balqis: Software, Investigation; M. A. Mukhlish: Software, Investigation; A. Altway: Conceptualization, Methodology, Supervision; M. Mahfud: Conceptualization, Methodology, Supervision. All authors have read and agreed to the published version of the manuscript.

References

[1] NASA (2022). Carbon Dioxide Concentration. https://climate.nasa.gov/vital-signs/carbon-dioxide. Accessed 31 Aug 2022.

[2] Chu, S., Majumdar, A. (2012). Opportunities and challenges for a sustainable energy future. *Nature*, 488(7411), 294–303. DOI: 10.1038/nature11475.

[3] Hegerl, G., Stott, P. (2014). From past to future warming. *Science*, 343(6173), 844–845. DOI: 10.1126/science.1249368.

Table 4. Comparison between MATLAB R2020a simulation result and industrial plant data.

Variable comparison	MATLAB	Industrial plant data
Pressure (bar)	1.86	1.86
Flow rate of rich amine solution (m^3.hour^{-1})	10	10
Temperature of rich amine solution (K)	358.15	358.15
Reboiler load (kJ/kg of CO_2)	60,606	60,606
CO_2 stripping efficiency (%)	88.35	89.68

[4] Rutgersson, A., Jaagus, J., Schenk, F., Stendel, M. (2014). Observed changes and variability of atmospheric parameters in the Baltic Sea region during the last 200 years. *Climate Research*, 61(2), 177–190. DOI: 10.3354/cr01244.

[5] Howard-Grenville, J., Buckle, S.J., Hoskins, B.J., George, G. (2014). Climate Change and Management. *Academy of Management Journal*, 57(3), 615–623. DOI: 10.5465/amj.2014.4003.

[6] Mondal, B.K., Bandyopadhyay, S.S., Samanta, A.N. (2015). Vapor-liquid equilibrium measurement and ENRTL modeling of CO_2 absorption in aqueous hexamethylenediamine. *Fluid Phase Equilibria*, 402, 102–112. DOI: 10.1016/j.fluid.2015.05.033.

[7] Borhani, T.N.G., Akbari, V., Afkhamipour, M., Hamid, M.K.A., Manan, Z.A. (2015). Comparison of equilibrium and non-equilibrium models of a tray column for post-combustion CO_2 capture using DEA-promoted potassium carbonate solution. *Chemical Engineering Science*, 122, 291–298. DOI: 10.1016/j.ces.2014.09.017.

[8] Nisa, N.I.F., Mahfud, M., Altway, A., Nurkhamidah, S., Eduard, W., Bethiana, T.N. (2021). Simulation for Absorption of Acid Gas into Piperazine Promoted Methyl Diethanolamine Solution Using Sieve Tray Column. *Journal of Physics: Conference Series*, 1845(1) DOI: 10.1088/1742-6596/1845/1/012003.

[9] Mahmoodi, L., Darvishi, P. (2017). Mathematical modeling and optimization of carbon dioxide stripping tower in an industrial ammonia plant. *International Journal of Greenhouse Gas Control*, 58, 42–51. DOI: 10.1016/j.ijggc.2017.01.005.

[10] Brickett, L., Munson, R., Litynski, J. (2020). U.S. DOE/NETL large pilot-scale testing of advanced carbon capture technologies. *Fuel*, 268(January), 117169. DOI: 10.1016/j.fuel.2020.117169.

[11] Khoshraftar, Z., Ghaemi, A. (2022). Presence of activated carbon particles from waste walnut shell as a biosorbent in monoethanolamine (MEA) solution to enhance carbon dioxide absorption. *Heliyon*, 8(1), e08689. DOI: 10.1016/j.heliyon.2021.e08689.

[12] Xu, X., Yang, Y., Acencios Falcon, L.P., Hazewinkel, P., Wood, C.D. (2019). Carbon capture by DEA-infused hydrogels. *International Journal of Greenhouse Gas Control*, 88(June), 226–232. DOI: 10.1016/j.ijggc.2019.06.005.

[13] Aghel, B., Sahraie, S., Heidaryan, E., Varmira, K. (2019). Experimental study of carbon dioxide absorption by mixed aqueous solutions of methyl diethanolamine (MDEA) and piperazine (PZ) in a microreactor. *Process Safety and Environmental Protection*, 131, 152–159. DOI: 10.1016/j.psep.2019.09.008.

[14] Kohl, A.L., Nielsen, R.B. (1997). *Gas Purification*. Gulf Publishing Company.

[15] Niknam, H., Jahangiri, A., Alishvandi, N. (2019). Removal of CO_2 from gas mixture by aqueous blends of monoethanolamine + piperazine and thermodynamic analysis using the improved kent eisenberg model. *Journal of Environmental Treatment Techniques*, 7(1), 158–165.

[16] Borhani, Babamohammadi, S., Khallaghi, N., Zhang, Z. (2022). Mixture of piperazine and potassium carbonate to absorb CO_2 in the packed column: Modelling study. *Fuel*, 308(April 2021), 122033. DOI: 10.1016/j.fuel.2021.122033.

[17] Kale, C., Tönnies, I., Hasse, H., Górak, A. (2011). Simulation of Reactive Absorption: Model Validation for CO_2-MEA system. *Computer Aided Chemical Engineering*, 29, 61–65. DOI: 10.1016/B978-0-444-53711-9.50013-4.

[18] Qi, G., Wang, S., Yu, H., Feron, P., Chen, C. (2013). Rate-based modeling of CO_2 absorption in aqueous NH3 in a packed column. *Energy Procedia*, 37(x), 1968–1976. DOI: 10.1016/j.egypro.2013.06.077.

[19] Rafagnim, N.Z., Barbieri, M.R., Noriler, D., Meier, H.F., Silva, M.K. da (2021). Euler–Euler model for CO_2-MEA reactive absorption on a sieve-tray. *Chemical Engineering Research and Design*, 170, 201–212. DOI: 10.1016/j.cherd.2021.03.033.

[20] Salem, A., Amanpour Reyhani, F. (2015). Applied aspects for enhanced CO_2 capture from reformer gas: Comparison between the performance of valve tray absorber and packed column, Part I. *International Journal of Greenhouse Gas Control*, 42, 237–245. DOI: 10.1016/j.ijggc.2015.07.028.

[21] Shahid, M.Z., Maulud, A.S., Bustam, M.A., Suleman, H., Abdul Halim, H.N., Shariff, A.M. (2021). Packed column modelling and experimental evaluation for CO_2 absorption using MDEA solution at high pressure and high CO_2 concentrations. *Journal of Natural Gas Science and Engineering*, 88(January), 103829. DOI: 10.1016/j.jngse.2021.103829.

[22] Oyenekan, B.A., Rochelle, G.T. (2009). Rate modeling of CO_2 stripping from potassium carbonate promoted by piperazine. *International Journal of Greenhouse Gas Control*, 3(2), 121–132. DOI: 10.1016/j.ijggc.2008.06.010.

[23] Nisa, N.I.F., Altway, A., Susianto, S. (2019). Simulasi Unit Stripping CO_2 Dalam Packed Column Skala Industri Dengan Kondisi Non-(Isothermal Simulation of Industrial Scale Column CO_2 Stripping Units With Non-Isothermal Conditions). *Jurnal Rekayasa Kimia & Lingkungan*, 14(1), 53–62, DOI: 10.23955/rkl.v14i1.13547.

[24] Park, H.M. (2014). A multiscale modeling of carbon dioxide absorber and stripper using the Karhunen-Loève Galerkin method. *International Journal of Heat and Mass Transfer*, 75, 545–564. DOI: 10.1016/j.ijheatmasstransfer.2014.03.089.

[25] Oyenekan, B.A., Rochelle, G.T. (2006). Energy performance of stripper configurations for CO 2 capture by aqueous amines. *Industrial and Engineering Chemistry Research*, 45(8), 2457–2464. DOI: 10.1021/ie050548k.

[26] Alie, C., Backham, L., Croiset, E., Douglas, P.L. (2005). Simulation of CO_2 capture using MEA scrubbing: A flowsheet decomposition method. *Energy Conversion and Management*, 46(3), 475–487. DOI: 10.1016/j.enconman.2004.03.003.

[27] Jassim, M.S., Rochelle, G.T. (2006). Innovative absorber/stripper configurations for CO 2 capture by aqueous monoethanolamine. *Industrial and Engineering Chemistry Research*, 45(8), 2465–2472. DOI: 10.1021/ie050547s.

[28] Tobiesen, F.A., Svendsen, H.F., Hoff, K.A. (2005). Desorber Energy Consumption Amine Based Absorption Plants. *International Journal of Green Energy*, 2(2), 201–215. DOI: 10.1081/ge-200058981.

[29] Tobiesen, F.A., Svendsen, H.F. (2006). Study of a modified amine-based regeneration unit. *Industrial and Engineering Chemistry Research*, 45(8), 2489–2496. DOI: 10.1021/ie050544f.

[30] Weiland, R.H., Rawal, M., Rice, R.G. (1982). Stripping of carbon dioxide from monoethanolamine solutions in a packed column. *AIChE Journal*, 28(6), 963–973. DOI: 10.1002/aic.690280611.

[31] Borhani, T.N.G., Oko, E., Wang, M. (2019). Process modelling, validation and analysis of rotating packed bed stripper in the context of intensified CO_2 capture with MEA. *Journal of Industrial and Engineering Chemistry*, 75, 285–295. DOI: 10.1016/j.jiec.2019.03.040.

[32] Lin, Y.J., Rochelle, G.T. (2014). Optimization of advanced flash stripper for CO_2 capture using piperazine. *Energy Procedia*, 63, 1504–1513. DOI: 10.1016/j.egypro.2014.11.160.

[33] Moioli, S., Pellegrini, L.A. (2013). Regeneration section of CO_2 capture plant by MEA scrubbing with a rate-based model. *Chemical Engineering Transactions*, 32, 1849–1854. DOI: 10.3303/CET1332309.

[34] Ariani, A., Chalim, A., Hardjono, H. (2021). Modeling and simulation of CO_2 gas desorption process in promoted MDEA solution using packed column. *IOP Conference Series: Materials Science and Engineering*, 1073(1), 012004. DOI: 10.1088/1757-899x/1073/1/012004.

[35] Rahimpour, M.R., Darvishi, P. (2007). Desorption Of Carbon Dioxide From Promoted Hot Potassium Carbonate In An Industrial Stripper Using Penetration Theory. *Chemical Technology An Indian Journal*, 2(1), 13–23.

[36] Garcia, M., Knuutila, H.K., Gu, S. (2017). ASPEN PLUS simulation model for CO_2 removal with MEA: Validation of desorption model with experimental data. *Journal of Environmental Chemical Engineering*, 5(5), 4693–4701. DOI: 10.1016/j.jece.2017.08.024.

[37] Yi, F., Zou, H.K., Chu, G.W., Shao, L., Chen, J.F. (2009). Modeling and experimental studies on absorption of CO_2 by Benfield solution in rotating packed bed. *Chemical Engineering Journal*, 145(3), 377–384. DOI: 10.1016/j.cej.2008.08.004.

[38] Khan, A.A., Halder, G., Saha, A.K. (2019). Kinetic effect and absorption performance of piperazine activator into aqueous solutions of 2-amino-2-methyl-1-propanol through post-combustion CO_2 capture. *Korean Journal of Chemical Engineering*, 36(7), 1090–1101. DOI: 10.1007/s11814-019-0296-9.

[39] Pudjiastuti, L., Susianto, Altway, A., Ic, M.H., Arsi, K. (2015). Kinetic study of carbon dioxide absorption into glycine promoted diethanolamine (DEA). *AIP Conference Proceedings*, 1699, 060011. DOI: 10.1063/1.4938365.

[40] Dash, S.K., Samanta, A., Nath Samanta, A., Bandyopadhyay, S.S. (2011). Absorption of carbon dioxide in piperazine activated concentrated aqueous 2-amino-2-methyl-1-propanol solvent. *Chemical Engineering Science*, 66(14), 3223–3233. DOI: 10.1016/j.ces.2011.02.028.

[41] Chakma, A., Meisen, A. (1990). Improved Kent-Eisenberg model for predicting CO_2 solubilities in aqueous diethanolamine (DEA) solutions. *Gas Separation and Purification*, 4(1), 37–40. DOI: 10.1016/0950-4214(90)80025-G.

[42] Altway, A., Susianto, S., Suprapto, S., Nurkhamidah, S., Nisa, N.I.F., Hardiyanto, F., Mulya, H.R., Altway, S. (2015). Modeling and simulation of CO_2 absorption into promoted aqueous potassium carbonate solution in industrial scale packed column. *Bulletin of Chemical Reaction Engineering & Catalysis*, 10(2), 111–124. DOI: 10.9767/bcrec.10.2.7063.111-124.

[43] Danckwerts, P.V. (1970). *Gas Liquid Reactions*. McGraw-Hill Book Company.

[44] Sander, R. (2015). Compilation of Henry's law constants (version 4.0) for water as solvent. *Atmospheric Chemistry and Physics*, 15(8), 4399–4981. DOI: 10.5194/acp-15-4399-2015.

[45] Weisenberger, S., Schumpe, A. (1996). Estimation of Gas Solubilities in Salt Solutions at Temperatures from 273 K to 363 K. *AIChE Journal*, 42(1), 298–300. DOI: 10.1002/aic.690420130.